IOP Publishing | Royal Swedish Academy of Sciences Physica Scripta
Phys. Scr. T171 (2020) 014024 (6pp) https://doi.org/10.1088/1402-4896/ab43fa

Sputtering of beryllium oxide by deuterium at various temperatures simulated with molecular dynamics

E A Hodille, J Byggmästar, E Safi and K Nordlund

Department of Physics, University of Helsinki, PO Box 43, FI-00014, Finland

E-mail: etienne.hodille@helsinki.fi

Received 4 June 2019, revised 19 August 2019
Accepted for publication 12 September 2019
Published 2 March 2020

Abstract

The sputtering yield of beryllium oxide (BeO) by incident deuterium (D) ions, for energies from 10 eV to 200 eV, has been calculated for temperatures between 300 K and 800 K using classical molecular dynamics. First, cumulative irradiations are carried out to build up a concentration of D in the material, equal to the experimentally measured concentration, that varies from an atomic fraction of 0.12 (300 K–500 K) to 0.02 (800 K). After building up the concentration of D, non-cumulative irradiations are carried out to estimate the sputtering yields of BeO. For all incident energies, the sputtering yield peaks at 500 K, being closely related to the decrease of the concentration of D above this temperature. At 10 eV, the concentration of D on the surface drives the temperature dependence, while above 30 eV, it is the amount of surface damage created during the cumulative irradiation.

Keywords: plasma-wall interactions, molecular dynamics, beryllium oxide, deuterium

(Some figures may appear in colour only in the online journal)

1. Introduction

Beryllium (Be) is the material chosen for the first wall of both JET [1, 2] and ITER [3]. Ions coming from the plasma can lead to sputtering of this material, reducing the lifetime of the plasma-facing components and creating a source of impurity for the plasma. In addition, the sputtered material can migrate in the edge plasma and be redeposited on surfaces, creating a deposited layer that is expected to be the main medium for fuel retention in ITER [4, 5]. It is thus important to estimate the sputtering of Be materials in a fusion environment.

Be oxidises easily, and a thin beryllium oxide (BeO) layer can be formed with a small pressure of oxygen. Thus, BeO layers can be formed between plasmas and quickly removed in a strong sputtering area during plasma operation (in limiter plasma, for instance). BeO can also be formed during off-normal events such as the melting of Be, as BeO inclusions have been observed by Raman spectroscopy in melted regions [6, 7]. The sputtering of BeO by deuterium (D) ions is thus of importance for the description and understanding of plasma–wall interactions.

In this work we use molecular dynamics (MD) to estimate the sputtering yields of BeO by D ions. In a previous study, MD was used to determine these sputtering yields at 300 K [8]. During tokamak operations, the temperature of the first wall can rise above 300 K. Here, the MD simulations have been extended to provide estimations of sputtering yields of BeO at up to 800 K.

2. Method

The irradiation of BeO was simulated with classical MD using the MD code PARCAS [9]. The simulation cells contain three species: beryllium (Be), oxygen (O), and deuterium (D). To describe the interactions between these species, Tersoff-like potentials [10, 11] have been used. For these interactions, D atoms are considered as H atoms with a mass of 2.014 atomic mass units. The Be-Be and Be-H potentials are both taken from [12] (version II), the H-H potential is taken from [13], the O-O is taken from [14], the Be-O is taken from [15], and the O-H part is taken from [8]. The full

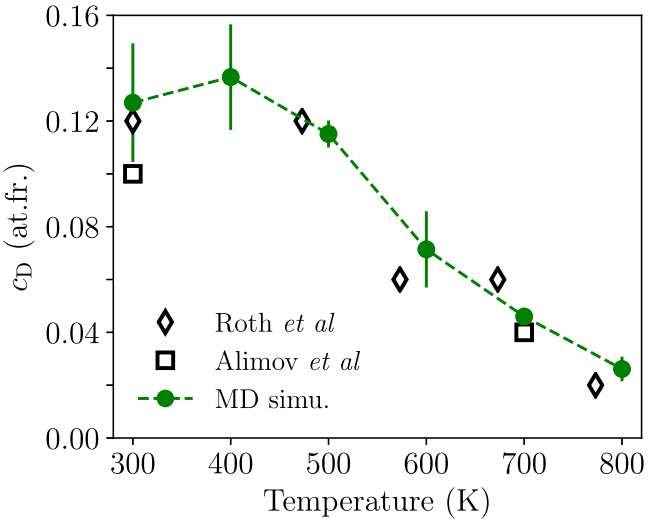

Figure 1. Evolution of the deuterium concentration, c_D, with temperature. The open symbols are the experimental values reported by Roth *et al* [17] and Alimov *et al* [18]. The closed circles are the values of the deuterium concentration, c_D, used in the MD simulations (averaged over all six energies used in this paper). The error bars are the standard deviations over all six energies.

Be-O-H potential was previously shown to give good agreement between simulated and experimental sputtering yields [8], and is therefore well-suited for plasma–wall interaction simulations.

In [8] it is shown that the sputtering yield increases with c_D (see below) in the material. The best comparison between MD and experimental sputtering yields is obtained at 300K for $c_D \approx 0.12$ atomic fraction (at.fr.), which is the saturation concentration of deuterium in BeO determined experimentally for irradiation at 300 K [16]. Thus, for the present simulations at different temperatures, the temperature-dependent values of c_D in BeO are also used. Roth *et al* [17] and Alimov *et al* [18] report those values of c_D for temperatures between 300K and 773 K. They are shown in figure 1. The two experimental studies agree on the evolution of c_D in BeO with temperature: c_D is about constant (equal to 0.12 at.fr.) from 300 K to 500 K, and then falls at temperatures above 500 K.

The simulation set-up used in this paper is the same as in [8]: a wurtzite BeO cell with a $(000\bar{1})$ surface is irradiated with ion energies of 10 eV, 30 eV, 50 eV, 80 eV, 140 eV and 200 eV. The irradiated temperatures are 400 K, 500 K, 600 K, 700 K and 800 K. The sputtering data at 300 K are taken from [8] and have been obtained with the exact same procedure. The cell is 25 × 24 Å^2 in the (x, y) plane and is elongated in the z direction (Z = 68 Å for $E_{inc} < 80$ eV and Z = 104 Å for $\geqslant 80$ eV). The duration of each irradiation is 7 000 fs and prior to any irradiation, the box is randomly shifted over the periodic boundaries in the x and y directions to simulate a uniform bombardment. More details on the simulation set-up (relaxation of the box, temperature control, incident angle) can be found in [8].

Firstly, as in [8], cumulative irradiations are run to build up a D-rich layer. The cumulative irradiations are stopped when the D concentration in this layer is comparable to the experimental concentrations. The values of c_D obtained during this first step are shown in figure 1 (averaged over the six energies). For the lowest temperatures, these concentrations are reached after about 100 impacts (for 10 eV) or 400 impacts (for 200 eV), while only a few tens of impacts are needed for the highest temperatures (lowest c_D). The cells obtained in this way and used in the non-cumulative irradiation are shown in figure 2 for incident energies of 10 eV, 50 eV and 140 eV for the different temperatures. For 30 eV (80 eV), the cells are similar to those obtained for 50 eV with more (fewer) D atoms on the surface. For 200 eV, the simulation cells are similar to those obtained for 140 eV, with a more pronounced swelling of the cell for the highest value of c_D. The D depth profiles are limited to the implantation zone (a few nm below the surface) as the diffusion coefficient of H in BeO is large [20, 21], meaning that no diffusion can be captured at the MD time scale.

After building up the relevant deuterium concentration in the material, 10 000 non-cumulative impacts are simulated to determine the sputtering yields of BeO, Y_{BeO}, calculated as the average number of sputtered Be and O atoms over incoming D ions. The standard deviations over all individual bombardments are used to provide error bars to the estimated sputtering yields. Again, to simulate a uniform bombardment, the simulation cell is randomly shifted over the periodic boundaries in the x and y directions before any impacts.

3. Results and discussion

3.1. Evolution of Y_{BeO} with the temperature

The sputtering yields calculated by MD for the various incident energies and temperatures are shown in figure 3 and are correlated to the evolution of c_D with temperature. Experimental data at room temperature on oxidized Be samples [22, 24] and sintered BeO [23] are also reported. For all energies, Y_{BeO} increases from 300 K to 500 K as c_D is constant, and as soon as c_D decreases, Y_{BeO} decreases as well. Such peaking of the sputtering yield with temperature has already been reported for carbon-based materials [25–27] and Si [25], and is understood to be evidence of chemical sputtering [27]. Concerning BeO, the evolution of sputtering yields with temperature has not been studied experimentally so far. However, concerning metallic Be, Nishijima *et al* [28] observed experimentally a decrease of the sputtering yield of a plasma-deposited Be layer between 320K and 570 K that they attributed to a decrease of the deuterium retention at 570 K. In addition, the sputtering yield of Be in JET has also been shown to decrease between 200 °C (473 K) and 400 °C (673 K) [29, 30]. This is explained by the decrease of c_D in Be with temperature, diminishing the production of BeD molecules as shown in MD simulations [31]. Thus, to investigate further the observed peaking of Y_{BeO} at 500 K, we distinguished the different sputtering products as follows: single O/Be atoms, BeD_z and OD_z molecules, Be_xO_y, $Be_xO_yD_z$ and O_2 molecules. For OD_z molecules, z is equal to 1 or 2 ($z = 2$

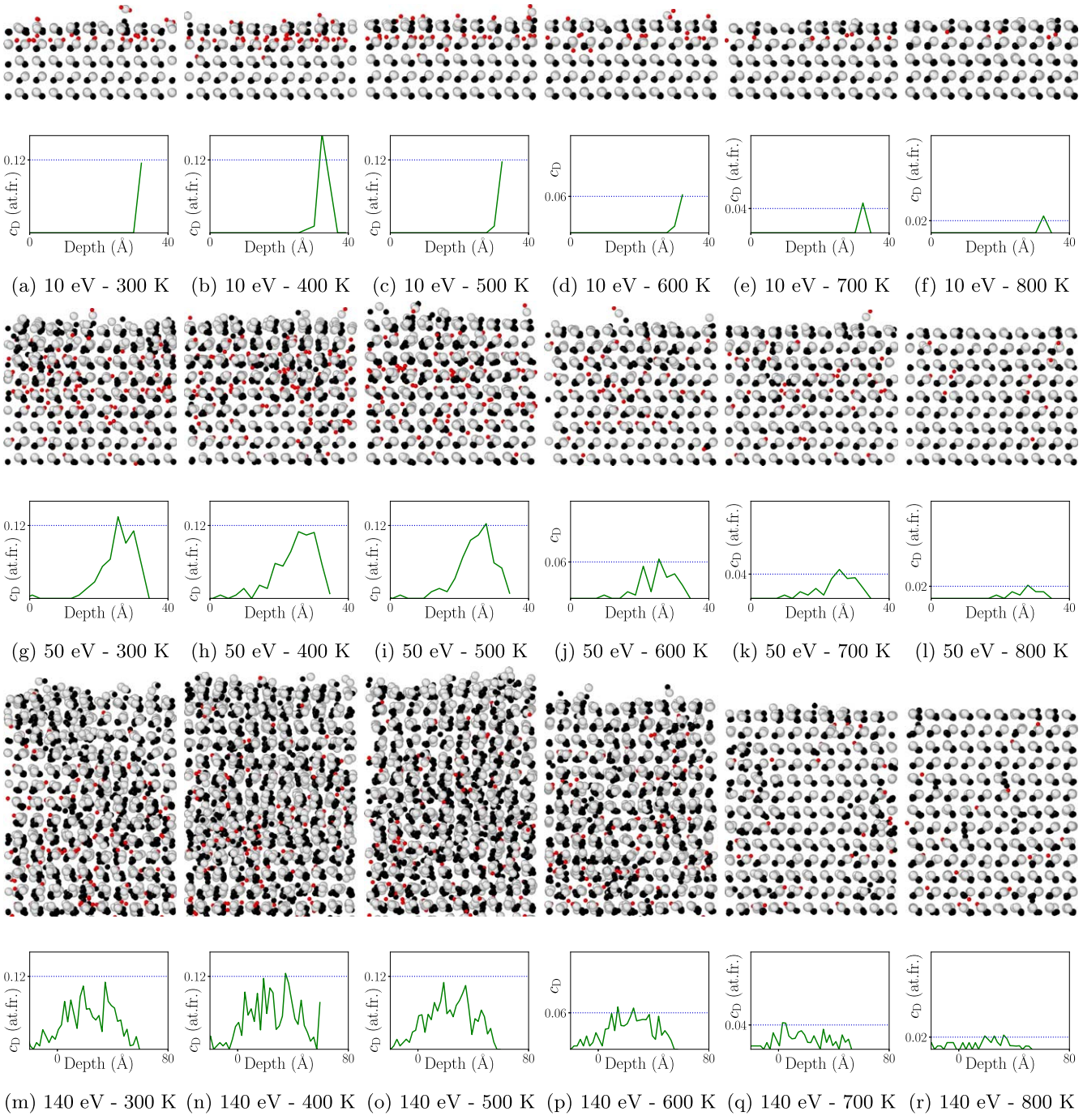

Figure 2. Simulation cells obtained by cumulative irradiation and used for non-cumulative irradiations for the different temperatures from 300 K to 800 K and incident energies of 10 eV ((a) to (f)), 50 eV ((g) to (l)) and 140 eV ((m) to (r)). Top: snapshot of the cells, obtained with OVITO software [19], with O atoms in grey, Be in black, and D in red. Bottom: evolution of c_D at the depth for the considered cells. The experimental concentrations are shown with a dotted line.

denotes heavy water molecules). The contribution of each of these products is shown in figure 3.

3.2. Physical sputtering of Be and O

The single atoms are produced through physical sputtering processes, and no strong temperature evolution can be determined for physical sputtering of Be and O. We note that at 30 eV, there is no single Be sputtered at 300 K, while there are at higher temperatures. The obtained sputtering yields of $\approx 1 \times 10^{-3}$ represent about 10 sputtering events among the 10 000 non-cumulative irradiations. Thus, the sputtering of a few Be atoms could have been missed by the limited number of impacts.

In figure 3, one can roughly estimate the threshold for physical sputtering of Be and O. It is between 10 eV and 30 eV for Be, while it is around 30 eV for O. This difference makes sense, considering the difference of mass between these two elements.

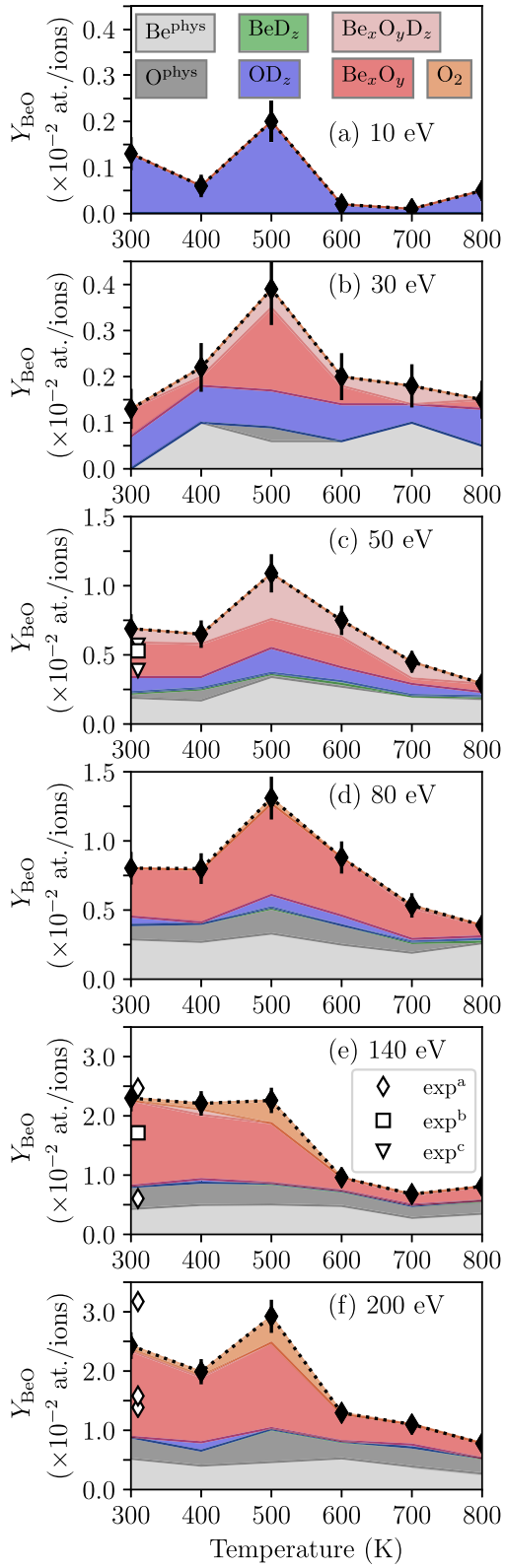

Figure 3. Evolution of the MD sputtering yield Y_{BeO} with temperature. The contributions of single Be atoms (Be^{phys}), single O atoms (O^{phys}), BeD_z, OD_z, Be_xO_y, $Be_xO_yD_z$ and O_2 are also shown. exp^a [22] (150 eV and 200 eV), exp^b [23] (50 eV and 150 eV) and exp^c [24] (50 eV and 60 eV).

3.3. Swift chemical sputtering of OD_z molecules

The BeD_z and OD_z molecules are mostly produced by swift chemical sputtering (SCS) [8, 32]. The proportion of BeD_z is a maximum of a few percent, while that of OD_z is 100% for 10 eV. The predominance of OD_z comes mostly from the fact that the OD dimer is much more stable than BeD [8].

For 10 eV, this contribution, which represents all the sputtering events, peaks at 500 K and then falls by one order of magnitude as c_D decreases. In [8] we showed that the SCS mechanism is active for $10\,eV < E_{inc} \leqslant 80\,eV$ for a perfect $(000\bar{1})$ surface. However, the presence of adsorbed D leads to the formation of O-D bonds, which loosen the bond of the O atoms to the rest of the material [8]. Such a bound O atom can then be sputtered by 10 eV D ions. The amount of O-D bonds on the surface for the highest values of c_D (300 K–500 K) is obviously higher (figures 2(a) to (c)) than for the lowest values of c_D (700 K–800 K). For 700 K and 800 K, no O-D bonds are actually on the surface and all the D atoms are below the surface (figures 2(e), (f)). For $E_{inc} \geqslant 30$ eV, the temperature dependence of the formation of OD_z through SCS is not as obvious, except for a slight increase from 400 K to 500 K at 50 eV. Indeed, other sputtering processes start to appear (physical sputtering, formation of $Be_xO_yD_z$ molecules). Thus, SCS leading to OD_z molecules contributes only a few tens of percentage points at 30 eV, a few percent at 50 eV and 80 eV, and almost zero above that, as the upper limit for this process is about 80 eV [8].

3.4. Sputtering of $Be_xO_yD_z$ molecules

In the Be-O potentials used here, the energy of the BeO dimer had to be overestimated by 1 eV/atom in order to have accurate cohesive energies for the bulk phases [15]. This could favor the formation of $Be_xO_yD_z$ molecules in our MD simulations that appear mostly as a BeO dimer and BeOD molecules. However, BeO, BeOD and BeO_2 molecules have been observed experimentally by mass spectrometry after the bombardment of Be samples by an $(Ar^+ + D_2^+)$ mixture [33]. Thus, their formation in our MD simulations is not an artifact of the potential.

For $E_{inc} \geqslant 30$ eV, as can be seen in figure 3, the temperature dependence of Y_{BeO} is mostly due to the sputtering of $Be_xO_y(D_z)$ molecules (including O_2). For most of the events involving $Be_xO_y(D_z)$ formation, the incident ion is not bound to the sputtered molecules: the initial interaction leading to the sputtering has a physical nature. It is the description of the chemically assisted physical sputtering (CAPS) suggested by Brezinsek *et al* [34]. In our previous simulations of irradiations of BeO at 300K, we determined four processes leading to the production of these molecules via CAPS. First, there are two types of BeO physical sputtering mechanisms (direct and delayed) called $Y^{phys}_{Be_xO_yD_z}$. During a direct physical sputtering event, the incident D ion physically sputters one Be/O atom, which drags with it one of its O/Be neighbors, forming a BeO dimer. During a delayed physical sputtering event, the incident D atom physically sputters one atom on its way in the material, is

back-scattered, and sputters another atom on its way back. If both sputtered atoms were neighbors, they might be sputtered together within a short space and time interval, allowing them to stay bound as a BeO dimer. (This is a rare event, due to the conditions required for it to happen.) Trajectories for both mechanisms can be found in [8]. Then, there are two other processes active only on damaged surfaces, i.e., surfaces containing roughness and loosely-bound groups of atoms (figure 2). The first is delayed SCS, during which an atom is kicked away from its initial position. It can then move on the surface and possibly interact with other atoms via the SCS mechanism, releasing molecules. The second is detachment-induced sputtering: on a damaged surface there are atoms or groups of atoms that are more loosely bound to the surface than any atoms on a pristine surface. If the incident D ion kicks away the atoms that bond a group of these atoms to the rest of the material, they can be detached from the surface. Trajectories for both mechanisms can also be found in [8]. Both processes are regrouped in $Y^{\mathrm{dam}}_{\mathrm{Be}_x\mathrm{O}_y\mathrm{D}_z}$.

For $c_{\mathrm{D}} \approx 0$ at.fr., with a perfect $(000\bar{1})$ surface, among these two processes, only $Y^{\mathrm{phys}}_{\mathrm{Be}_x\mathrm{O}_y\mathrm{D}_z}$ is active and it represents about 30 percent of the total sputtering yield [8]. In figure 3, for 700K and 800 K ($c_{\mathrm{D}} < 0.04$ at.fr.), the contribution of $\mathrm{Be}_x\mathrm{O}_y(\mathrm{D}_z)$ is also about 30 percent and the irradiated surfaces are almost perfect $(000\bar{1})$ (figure 2). Thus, at these temperatures, only $Y^{\mathrm{phys}}_{\mathrm{Be}_x\mathrm{O}_y\mathrm{D}_z}$ is active.

On the other hand, for the highest values of c_{D} (300 K to 600 K), as seen in figure 2, the material is more damaged (and eventually amorphized). This amorphization and surface damage are expected in insulator material [35]: the energy threshold for this amorphization can be very low (about 0.01 keV/target atom) for materials that are more covalent than ionic [35], as is the case with BeO [36]. Thus, it activates $Y^{\mathrm{dam}}_{\mathrm{Be}_x\mathrm{O}_y\mathrm{D}_z}$ for the highest values of c_{D}, for which $Y_{\mathrm{Be}_x\mathrm{O}_y\mathrm{D}_z}$ contributes 30–70 percent of the total sputtering yield. As a larger amount of irradiation is needed to build up the relevant value of c_{D}, the surfaces for higher c_{D} values are more damaged than for low c_{D} values. Thus, the decrease of c_{D} above 500 K induces a reduced amount of surface damage, leading to a decrease of $Y^{\mathrm{dam}}_{\mathrm{Be}_x\mathrm{O}_y\mathrm{D}_z}$ and hence also Y_{BeO} from 500 K to 800 K.

Despite $c_{\mathrm{D}}(300\ \mathrm{K}) > c_{\mathrm{D}}(600\ \mathrm{K})$, for $30\ \mathrm{eV} \leqslant E_{\mathrm{inc}} \leqslant 80\ \mathrm{eV}$, there is $Y_{\mathrm{BeO}}(600\ \mathrm{K}) > Y_{\mathrm{BeO}}(300\ \mathrm{K})$, a pronounced increase of Y_{BeO} from 300 K to 500 K and a smooth decrease above 500 K. It means a thermally activated process either: (i) increases the amount of surface damage when building up c_{D}, or; (ii) facilitates the sputtering of atoms due to the thermal motion. Both can play a role in the temperature behavior of Y_{BeO} but one can expect that the enhancement of Y_{BeO} by a higher thermal motion would be similar for any incident energies. As the peaking is observed only for $E_{\mathrm{inc}} \leqslant 80$ eV, it is most likely that the peaking of Y_{BeO} is due to a increase of the surface damage with the temperature (for a constant c_{D}). Indeed, the depth profiles in figure 2 show that the D atoms are deposited much closer to the surface at 50 eV: the damage is closer to (and eventually on) the surface. At 140 eV, the D atoms are much deeper in the bulk. Even though the damage induced by the irradiations increases from 300 K to 500 K, they are mostly located in the bulk and do not greatly affect the surface and the sputtering yield. Thus, for all energies, the disorder and damage induced by the ion irradiations increases with the temperature (from 300 K to 500 K), but they affect the sputtering yield in that range of temperature only if they are close to the surface. This difference in deposition also leads to higher surface D concentrations at low energy, especially for 30 eV and 50 eV, leading to a higher relative contribution of $\mathrm{Be}_x\mathrm{O}_y\mathrm{D}_z$ in the total sputtering yield.

Finally, one can note that O_2 is formed in a high fraction only at 500 K for $E_{\mathrm{inc}} \geqslant 140$ eV (figure 3). For these energies, the morphology of the surface damage (figure 2, (m) to (r)) favor delayed SCS. O_2 can then be formed if one O atom migrating on the surface recombines with another. The surface damage for $E_{\mathrm{inc}} \geqslant 140$ eV can also lead to the formation of adsorbed O_2 molecules as two O atoms are close together (one of their common Be neighbors being sputtered away during the cumulative irradiation). These O_2 molecules can be outgassed by the local increase of temperature created by the incident D ion impact. As the surface disorders are the highest at 500 K, and as outgassing is also favored by higher temperature, this explains the high fraction of O_2 production at 500 K.

4. Conclusions

MD simulations of the irradiation of a $(000\bar{1})$ wurtzite BeO surface at energies from 10 eV to 200 eV and at temperatures from 300 K to 800 K have been carried out to estimate the variation of the BeO sputtering yield Y_{BeO} with temperature. First, cumulative irradiations were carried out to build a concentration of deuterium, c_{D}, in the material. From experimental results, the value of c_{D} depends on the irradiation temperature [17, 18]: it is 0.12 at.fr. from 300K to 500 K and it then falls to 0.02 at.fr. at 800 K. In the simulations, for all energies, Y_{BeO} follows the trends of $c_{\mathrm{D}}(T)$ above 500 K: it decreases as the concentration of deuterium decreases. In the temperature range where c_{D} is constant, equal to 0.12 at.fr. (300 K–500 K), Y_{BeO} increases. For 10 eV, only OD_z molecules are sputtered and the decrease of Y_{BeO} with temperature/c_{D} is due to a decrease of the amount of O-D bonds on the surface, as these bonds decrease the binding energy of the O atom to the rest of the material. Above 30 eV, the variation of Y_{BeO} with temperature is mainly due to the evolution of the sputtering of $\mathrm{Be}_x\mathrm{O}_y\mathrm{D}_z$ molecules due to the change in surface damage; as c_{D} decreases, the amount of surface damage decreases as well as Y_{BeO}.

Acknowledgments

The work was perfomed under EUROfusion WP PFC. This work has been carried out within the framework of the EUROfusion Consortium and has received funding from Euratom research and training programmes 2014-2018 and 2019-2020 under grant agreement No. 633053. The views and opinions expressed herein do not necessarily reflect those of the European Commission. Grants of computer capacity from CSC-IT Center for Science and the Finnish Grid and Cloud Infrastructure (persistent identifier urn:nbn:fi:research-infras-2016072533) are gratefully acknowledged.

ORCID iDs

E A Hodille https://orcid.org/0000-0002-0859-390X
J Byggmästar https://orcid.org/0000-0002-4898-6150
E Safi https://orcid.org/0000-0002-4786-5234
K Nordlund https://orcid.org/0000-0001-6244-1942

References

[1] Philipps V, Mertens P, Matthews G F and Maier H 2010 Overview of the JET ITER-like wall project *Fusion Eng. Des.* **85** 1581–6 Proc. of the Ninth International Symposium on Fusion Nuclear Technology
[2] Brezinsek S 2015 Plasma-surface interaction in the be/w environment: Conclusions drawn from the JET-ILW for ITER *J. Nucl. Mater.* **463** 11–21 PLASMA-SURFACE INTERACTIONS 21
[3] Loarte A *et al* (the ITPA Scrape-off Layer, and Divertor Physics Topical Group) 2007 ch 4: Power and particle control *Nucl. Fusion* **47** S203
[4] Brezinsek S *et al* (JET EFDA contributors) 2013 Fuel retention studies with the ITER-like wall in JET *Nucl. Fusion* **53** 083023
[5] Heinola K *et al* 2015 Fuel retention in JET ITER-like wall from post-mortem analysis *J. Nucl. Mater.* **463** 961–5 PLASMA-SURFACE INTERACTIONS 21
[6] Kumar M *et al* (JET contributors) 2018 Identification of BeO and BeO_xD_y in melted zones of the JET Be limiter tiles: Raman study using comparison with laboratory samples *Nuclear Materials and Energy* **17** 295–301
[7] Makepeace C *et al* (J.E.T. Contributors) 2019 The effect of beryllium oxide on retention in JET ITER-like wall tiles *Nuclear Materials and Energy* **19** 346–51
[8] Hodille E A, Byggmästar J, Safi E and Nordlund K 2019 Molecular dynamics simulation of beryllium oxide irradiated by deuterium ions: sputtering and reflection *J. Phys. Condens. Matter* **31** 185001
[9] Nordlund K, Ghaly M, Averback R S, Caturla M, Diaz de la Rubia T and Tarus J 1998 Defect production in collision cascades in elemental semiconductors and fcc metals *Phys. Rev.* B **57** 7556–70
[10] Tersoff J 1986 New empirical model for the structural properties of silicon *Phys. Rev. Lett.* **56** 632–5
[11] Tersoff J 1988 New empirical approach for the structure and energy of covalent systems *Phys. Rev.* B **37** 6991–7000
[12] Björkas C, Juslin N, Timko H, Vörtler K, Nordlund K, Henriksson K and Erhart P 2009 Interatomic potentials for the Be-C-H system *J. Phys. Condens. Matter* **21** 445002
[13] Brenner D W 1990 Empirical potential for hydrocarbons for use in simulating the chemical vapor deposition of diamond films *Phys. Rev.* B **42** 9458–71
[14] Erhart P, Juslin N, Goy O, Nordlund K, Müller R and Albe K 2006 Analytic bond-order potential for atomistic simulations of zinc oxide *J. Phys. Condens. Matter* **18** 6585
[15] Byggmästar J, Hodille E A, Ferro Y and Nordlund K 2018 Analytical bond order potential for simulations of BeO 1D and 2D nanostructures and plasma–surface interactions *J. Phys. Condens. Matter* **30** 135001
[16] Roth J, Doerner R, Baldwin M, Dittmar T, Xu H, Sugiyama K, Reinelt M, Linsmeier C and Oberkofler M 2013 Oxidation of beryllium and exposure of beryllium oxide to deuterium plasmas in PISCES B *J. Nucl. Mater.* **438** S1044–7 Proc. of the XX International Conf. on Plasma-Surface Interactions in Controlled Fusion Devices
[17] Roth J, Wampler W R, Oberkofler M, van Deusen S and Elgeti S 2014 Deuterium retention and out-gassing from beryllium oxide on beryllium *J. Nucl. Mater.* **453** 27–30
[18] Alimov V K and Zakharov A P 2000 *Deuterium Retention In Beryllium and Beryllium Oxide* (Berlin: Springer) pp 247–64
[19] Stukowski A 2010 Visualization and analysis of atomistic simulation data with OVITO – the open visualization tool *Modell. Simul. Mater. Sci. Eng.* **18** 015012
[20] Hodille E A, Ferro Y, Piazza Z and Pardanaud C 2018 Hydrogen in beryllium oxide investigated by DFT: on the relative stability of charged-state atomic versus molecular hydrogen *J. Phys. Condens. Matter* **30** 305201
[21] Fowler J D, Dipankar C, Elleman T S, Payne A W and Verghese K 1977 Tritium diffusion in $A1_2O_3$ and BeO *J. Am. Ceram. Soc.* **60** 155–61
[22] Hirooka Y, Won J, Boivin R, Sze D and Neumoin V 1996 Effect of impurities on the erosion behavior of beryllium under steady-state deuterium plasma bombardment *J. Nucl. Mater.* **228** 148–53
[23] Roth J, Bohdansky J, Blewer R S, Ottenberger W and Borders J 1979 Sputtering of Be and BeO by light ions *J. Nucl. Mater.* **85-86** 1077–9
[24] Roth J, Eckstein W and Bohdansky J 1989 Beryllium self-sputtering: an interpolation of data for D, He, Ne and Ar *J. Nucl. Mater.* **165** 199–204
[25] Balden M and Roth J 2000 Comparison of the chemical erosion of Si, C and SiC under deuterium ion bombardment *J. Nucl. Mater.* **279** 351–5
[26] Schlüter M, Hopf C, Schwarz-Selinger T and Jacob W 2008 Temperature dependence of the chemical sputtering of amorphous hydrogenated carbon films by hydrogen *J. Nucl. Mater.* **376** 33–7
[27] Salonen E, Nordlund K, Keinonen J and Wu C H 2001 Swift chemical sputtering of amorphous hydrogenated carbon *Phys. Rev.* B **63** 195415
[28] Nishijima D, Doerner R P, Baldwin M J and De Temmerman G 2009 Erosion yields of deposited beryllium layers *J. Nucl. Mater.* **390-391** 132–5 Proc. of the XVIII International Conf. on Plasma-Surface Interactions in Controlled Fusion Device
[29] Brezinsek S, Stamp M F, Nishijima D, Borodin D, Devaux S, Krieger K, Marsen S, O'Mullane M, Björkas C, Kirschner A and (JET EFDA contributors) 2014 Study of physical and chemical assisted physical sputtering of beryllium in the JET ITER-like wall *Nucl. Fusion* **54** 103001
[30] Brezinsek S *et al* 2015 Beryllium migration in JET ITER-like wall plasmas *Nucl. Fusion* **55** 063021
[31] Safi E, Valles G, Lasa A and Nordlund K 2017 Multi-scale modelling to relate beryllium surface temperature, deuterium concentration and erosion in fusion reactor environment *J. Phys. D: Appl. Phys.* **50** 204003
[32] Björkas C, Borodin D, Kirschner A, Janev R K, Nishijima D, Doerner R and Nordlund K 2013 Molecules can be sputtered also from pure metals: sputtering of beryllium hydride by fusion plasma–wall interactions *Plasma Phys. Controlled Fusion* **55** 074004
[33] Ashida K, Matsuyama M, Watanabe K, Kawamura H and Ishitsuka E 1994 Secondary ion emission from beryllium surfaces by ar and/or (Ar + D_2) mixed ion bombardments *J. Nucl. Mater.* **210** 233–8
[34] Brezinsek S, Pospieszczyk A, Sergienko G, Dux R, Cavedon M, Faitsch M and Krieger K 2019 Chemically assisted physical sputtering of tungsten: identification via the 66+. transition of wd in textor and asdex upgrade plasmas *Nuclear Materials and Energy* **18** 50–5
[35] Hobbs L W 1994 Topology and geometry in the irradiation-induced amorphization of insulators *Nucl. Instrum. Methods Phys. Res., Sect. B* **91** 30–42
[36] Allouche A and Ferro Y 2015 First-Principles study of hydrogen retention and diffusion in beryllium oxide *Solid State Ionics* **272** 91–100